IET Nanobiotechnology

Research Article

IET Journals
The Institution of Engineering and Technology

Superparamagnetic cobalt ferrite nanoparticles as T_2 contrast agent in MRI: in vitro study

ISSN 1751-8741
Received on 17th June 2019
Revised 28th February 2020
Accepted on 11th March 2020
E-First on 3rd June 2020
doi: 10.1049/iet-nbt.2019.0210
www.ietdl.org

Zahra Mohammadi[1], Neda Attaran[2], Ameneh Sazgarnia[1], Seyed Ali Mousavi Shaegh[3,4], Alireza Montazerabadi[1] ✉

[1]*Medical Physics Research Center, Mashhad University of Medical Sciences, Mashhad, Iran*
[2]*Department of Medical Nanotechnology, Applied Biophotonics Research Center, Science and Research Branch, Islamic Azad University, Tehran, Iran*
[3]*Orthopedic Research Center, Mashhad University of Medical Sciences, Mashhad, Iran*
[4]*Clinical Research Unit, Ghaem Hospital Mashhad University of Medical Sciences, Mashhad, Iran*
✉ *E-mail: alireza.montazerabadi@gmail.com*

Abstract: Superparamagnetic cobalt ferrite nanoparticles ($CoFe_2O_4$) possess favourite advantages for theranostic applications. Most of previous studies reported that $CoFe_2O_4$ magnetic nanoparticles (MNPs) are suitable candidates for induction of hyperthermia and transfection agents for drug delivery. The present study synthesized and investigated the potential use of $CoFe_2O_4$ as a contrast agent in magnetic resonance imaging (MRI) by using a conventional MRI system. The $CoFe_2O_4$ were synthesized using co-precipitation method and characterized by TEM, XRD, FTIR, EDX and VSM techniques. Relaxivities r_1 and r_2 of $CoFe_2O_4$ were then calculated using a 1.5 Tesla clinical magnetic field. The cytotoxicity of $CoFe_2O_4$ was evaluated by the MTT assay. Finally, the optimal concentrations of MNPs for MRI uses were calculated through the analysis of T_2 weighted imaging cell phantoms. The superparamagnetic CoFe2O4 NPs with an average stable size of 10.45 nm were synthesized. Relaxivity $r_{1,2}$ calculations resulted in suitable r_2 and r_2/r_1 with values of 58.6 and 51 that confirmed the size dependency on relaxivity values. The optimal concentration of MNPs for MR image acquisition was calculated as 0.154 mM. Conclusion: $CoFe_2O_4$ synthesized in this study could be considered as a suitable T_2 weighted contrast agent because of its high r_2/r_1 value.

1 Introduction

Magnetic nanoparticles (MNPs) have been widely employed for various applications including magnetic resonance imaging (MRI), cancer hyperthermia, drug delivery, tissue imaging [1, 2]. Ferrite-based MNPs have been widely-explored as magnetic nanomaterials because of their excellent magnetic properties and multifunctional agents [3, 4]. Because of superparamagnetic properties of some ferrite-based nanoparticles, they have been largely employed to enhance the proton relaxivity for improved contrast and sensitivity of MR image acquisition [5]. In addition, ferrite-based MNPs could enhance the efficiency of hyperthermia owing to their high anisotropy, making them suitable candidates for theranostic applications. [6]. Among various ferrite-based MNPs, cobalt ferrite ($CoFe_2O_4$) nanoparticles have been recognised as a favourite contrast agent. They have hard magnetic material properties such as high saturation magnetisation, strong anisotropy and mechanical hardness [7]. Size and nanostructure of MNPs affect their magnetic properties that could be highly modulated by the preparation methods [8]. Water-soluble ferrite MNPs could be synthesised by a co-precipitation method for the biological applications [9]. Ferrite-based MNPs are used as contrast agents for T_2-weighted MR images. Based on theoretical models and experimental reports, r_2 relaxivity depends on the particles size and aggregation, the square of the saturation magnetisation and the applied magnetic field strength [10]. For small MNPs, which satisfy the motional averaging regime (MAR), $\Delta\omega\tau D < 1$, the outer sphere theory $\left(R = (16/45) f\,(\Delta\omega)\tau D\,\alpha\, d^2 Hyd\right)$ could be applied. This theory is not applicable for larger sizes of MNPs. The static dephasing regime is dominant for too large sizes. In this regard, r_2 enhances as size increases [2, 11]. According to Ta *et al.* [12] r_2 relaxivity increased as magnetic field strength enhanced from 1.5 to 9.4 T and then decreased. r_2/r_1 is an indicator of MRI efficiency that increases with the increment of field strength [13]. Some studies evaluated $CoFe_2O_4$ MNPs as MR contrast agent in different sizes and various magnetic fields, confirming the above-mentioned content [2, 14–17]. The studies indicated that high r_2/r_1 was obtained in large sizes and high magnetic fields. For clinical applications of superpramagnetic $CoFe_2O_4$, it is necessary to obtain high r_2 and r_2/r_1 in conventional MRI systems. A contrast agent with optimal efficiency within the range of clinical magnetic field might find clinical applications. In this study, the superparamagnetic $CoFe_2O_4$ MNPs were synthesised with high size stability, and characterised by high r_2/r_1 in clinical magnetic field strength. In addition, the cytotoxicity of this multifunctional agent was evaluated.

2 Material and methods

2.1 Materials

Co (II) and Fe (III) were purchased from Aldrich, Scharlau and Alfa Aesar. NaOH was obtained from Merck. MTT (3-(4, 5-Dimethylthiazol-2-yl)-2, 5-diphenyltetrazolium Bromide) was purchased from Sigma Aldrich. Agarose gel and deionised water (DI water) were used during the tests.

2.2 Preparation of $CoFe_2O_4$ MNPs

$CoFe_2O_4$ MNPs were synthesised by co-precipitation method in an alkaline aqueous environment. The reaction mixture was prepared from iron sulphate ($Fe_2(SO_4)_3$ salts) and cobalt chloride ($CoCl_2$ salt) with 0.1 M concentration of metal salts. All components of the reaction mixture were deoxygenated with nitrogen gas before mixing. In the next step, 5.0 M NaOH solution was added with vigorously stirring of mixing reaction until reaching a pH of 12.4. The obtained solution was then replaced while stirring at 80°C for

3 h under continuous nitrogen gas bubbling. Finally, the obtained sedimentary solution was centrifuged at 8500 rpm for 3 min, and was carefully rinsed 3 times using 10 ml of DI water. The sediment was then rinsed with ethanol. Afterwards, $CoFe_2O_4$ MNPs were dried at 50°C in dry heat [18].

2.3 Characterisation

2.3.1 Transmission electron microscopy (TEM): TEM was carried out to evaluate the morphology and size distribution of the synthesised particles. A 200 keV field emission Tecnia F 20 (FE) TEM was used to get a high-resolution TEM (HRTEM) and selected area (electron) diffraction (SAED) pattern. The particle size histogram was determined by measuring the diameter of ∼508 NPs and fitted by a Gaussian distribution.

2.3.2 Scanning electron microscopy (SEM): SEM was carried out to evaluate the morphology and surface structure of the MNPs. A 20 kV High Voltage MIRA3 TESCAN in 1.38 µm of the field of view was used for SEM.

2.3.3 Phase structure: The X-ray diffraction (XRD) indicated $CoFe_2O_4$ MNPs with crystal lattice structures. The data was collected at the room temperature on an X-ray diffractometer (GNR EXPLORER, ITALY). The Pure $CoFe_2O_4$ MNPs was obtained at a calcination temperature of 550°C [19]. The XRD system was run at 40 kV and 30 mA in a 2θ range of 20°–80°. In the present study, dimensions of $CoFe_2O_4$ MNPs crystal (D) were estimated using the XRD information through the Sherrer's equation.

2.3.4 Infrared spectra: Fourier-transform IR (FTIR) spectroscopy was used to identify functional groups and chemical structural changes in materials. For preparation of sample: the powder sample and KBr salt were ground to reduce the particles size. Then, a small amount of powder sample (about 0.1–2% of the KBr amount) was mixed with the KBr powder. Subsequently, the mixture was ground for 3–5 min. Uniformly fine-grained powders were prepared using milling the mixture using a mechanical vibrator or a mill. A thin and transparent pellet was obtained under pressure. Then, the pellet was put onto the sample holder in the FTIR system. The infrared spectrum was recorded by FTIR spectrometer (AVATAR 370 FT-IR Thermo Nicolet Spectrum) that operated at room temperature. It was performed by 64 scans and the samples were analysed in transmittance mode [20]. The Spectral resolution of the system was set at 4 cm^{-1} [21].

2.3.5 Energy dispersive X-Ray spectroscopy (EDS or EDX) spectrum: EDX spectrum indicated the presence of Fe, Co and O elements for the elemental analysis or chemical characterisation of samples.

2.3.6 Magnetometry: A vibrating sample magnetometer (vibrating sample magnetometer) VSM (manufactured by Danesh Pajoush Magnetis Company of Kashan, VSMF model, Iran) was used to measure the magnetic field-dependent magnetisation loop from −15,000 to 15,000 Oe at room temperature.

2.4 Relaxometry

Contrast agents in MRI could change relaxation times in tissues of interest. They can reduce T_1 and T_2 relaxation times that can be introduced as positive or negative contrast agents in MR images, respectively. $CoFe_2O_4$ MNPs are often used to enhance T_2 contrast are referred to as T_2 weighted images. T_2 and r_2 of water protons through the synthesised $CoFe_2O_4$ MNPs were calculated at 1.5 T MRI scanner (Avanto/Siemens. Kamyab Hospital). An in vitro phantom containing $CoFe_2O_4$ MNPs with various concentrations of 0.03, 0.04, 0.8, 0.12, 0.21, 0.25, 0.31, 0.36 and 0.42 mM was used to measure r_1 and r_2 values. All curve fitting routines, which were used to determine relaxation rate maps, were performed by Excel and R Software. T_1-weighted image was acquired at TE: 8.7 ms; TR1/TR2/TR3/TR4/TR5/TR6: 100/300/600/900/1200/2000 ms; flip angle: 20°; matrix: 256 × 192; the field of view: 260 mm; 100%; averages: 1, echo train length: 1; slice thickness:5 mm. T_2-weighted images were obtained by a T_2 spin-echo multisection pulse sequence with fixed repetition time (TR) of 2000 ms; TE1/TE2/TE3/TE4/TE5/TE6/TE7/TE8/TE9/TE10/TE11/TE12/ TE13/TE14/TE15/ TE16/:13.8/27.6/41.4/55.2/69/82.8/96.6/110.4/124.2/138/151/165.6 /179.4/193.2/207/220.8, flip angle: 20°; matrix: 256 × 192; field of view: 260 mm; 100%; averages: 1, echo train length: 1.

2.5 In-vitro MR imaging of cell phantoms

In vitro experiments were performed using KYSE 30 (RRID: CVCL1351), an oesophagus cancer cell line (CCLE) from Homo sapiens (Human), extracted from a 64-year-old man. KYSE 30 cells were seeded at a density of 2×10^6 at T12.5 culture flasks. After 24 h, different concentrations of $CoFe_2O_4$ composite 0.04, 0.8, 0.12, 0.21, 0.25, 0.31 mM) were added to the culture flasks. Culture flasks were then rinsed by PBS. The cells were then detached and centrifuged at a microtube (2 cc). Few drops of agarose gel were added to every microtube to fix cells followed by sonication to remove air bubbles. MR imaging of cell phantoms was performed for two times using a 1.5 T MRI system (Avanto/ SIEMENS. KAMYAB HOSPITAL). A T_2-Tse-cor gradient-echo sequence was acquired using the following sequence parameters: TR: 4000 ms, TE: 81 ms; flip angle: 20°; matrix: 256 × 192 interpolated; the field of view: 260 mm; averages: 1, echo train length: 1; slice thickness: 8 mm; 4 slices. The signal intensity (SI) was obtained from different concentrations of MNPs using Radiant Software (4.6.8 evaluation version) in cell phantoms. Percentage of ΔSI (($SI/SI_{Control}$) × 100) was calculated in which $SI_{Control}$ refers to cell phantom without MNPs.

2.6 Cytotoxicity of $CoFe_2O_4$MNPs

KYSE 30 was seeded at a density of 10^4 cells/well in a 96 well plate and incubated at 37°C for a doubling time of KYSE30 cell line for sufficient growth. $CoFe_2O_4$ MNPs in concentrations of 0.05, 0.1, 0.2, 0.3, 0.4, 0.5, 0.75 and 1 mM were separately added to microwells. Cells were then incubated for 24 h. Finally, MTT (3-(4, 5-Dimethylthiazol-2-yl)-2, 5-diphenyltetrazolium Bromide) test was performed to determine the cell death percentage.

3 Results

3.1 XRD pattern

Fig. 1 shows the obtained XRD result of $CoFe_2O_4$ MNPs. The XRD profile from $CoFe_2O_4$ MNPs, prepared by co-precipitation method, revealed the maximum XRD peak occurred at 2θ value of 35.87° that represented a typical $CoFe_2O_4$ with an interlayer spacing value of 3.83242 A. The structural analysis of XRD pattern indicated that $CoFe_2O_4$ MNPs had an inverse cubic spinel-type. Mean size of crystals (D) was estimated by the Sherrer's equation: $D = K\lambda/\beta \cos\theta$ where K is the Scherrer constant (0.94), λ is the wavelength, β is the FWHM (in radians), and θ is the peak angular position. Consequently, the size of the $CoFe_2O_4$ crystal was calculated by the most intensive peak (311) with a value of 11.67 nm [1, 2, 22–24]. The peaks of (111), (220), (311), (400), (511), and (440) were the main peaks of the typical inverse cubic $CoFe_2O_4$ MNPs XRD spectrum [25–28]. The peak (311) was used to obtain the lattice constant (a) of $CoFe_2O_4$ MNPs according to the following equation [29]:

$$a = d_{hkl}\sqrt{h^2 + k^2 + l^2}$$

where d_{hkl} is an interplanar distance; h, k and l refer to Miller indices and the lattice constant. The constant (a) of $CoFe_2O_4$

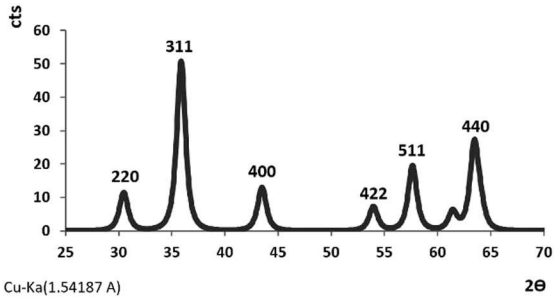

Fig. 1 *XRD pattern of sample $CoFe_2O_4$ synthesised by a co-precipitation method. The XRD system acted at 40 kV and 30 mA in a 2θ range of 20–80 [26, 30]*

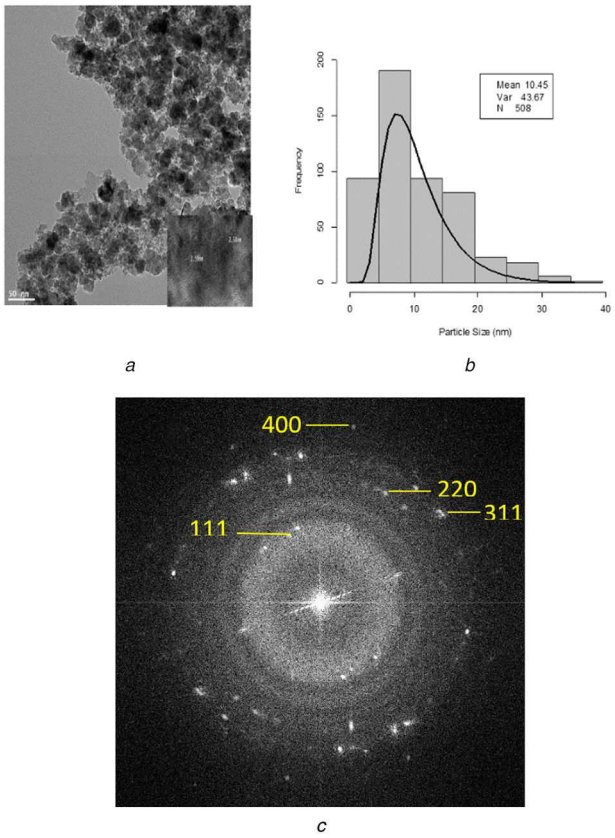

Fig. 2 *HRTEM images of $CoFe_2O_4$ MNPs*

(a) HRTEM of $CoFe_2O_4$ MNPs, ***(b)*** Size distribution histogram of $CoFe_2O_4$ MNPs with Gaussian distribution, ***(c)*** SAED pattern of $CoFe_2O_4$ MNPs [31, 32]

crystal was computed according to the peak (31 1) with a value of 0.83 nm.

3.2 High-resolution TEM

Fig. 2*a* shows the HRTEM image of $CoFe_2O_4$ MNPs. It is clear that $CoFe_2O_4$ MNPs synthesise were aggregated and had non-uniform shapes. Fig. 2*b* shows the nanoparticle size distribution in the histogram. Size distribution was determined by measuring the mean diameter of about 508 particles on HRTEM image. The average size was 10.45 nm that was fitted by a Gaussian distribution. The SAED pattern (Fig. 2*c*) shows at least four well-defined diffraction rings. The rings were indexed with estimating their d-spacing as (111), (311), (220) and (400) reflections of the cubic $CoFe_2O_4$ MNPs that are in agreement with the XRD results.

3.3 SEM

Fig. 3 shows the SEM image of $CoFe_2O_4$ MNPs that used to confirm the morphology of the synthesised MNPs. The obtained results show that $CoFe_2O_4$ MNPs had non-uniform shape. The average size was estimated as 25.6 nm using SEM analysis. Size estimation was performed by ImageJ software.

3.4 VSM

Magnetic properties of the synthesised $CoFe_2O_4$ MNPs were evaluated using a SQUID system. Magnetic hysteresis curves of MNPs were obtained at the magnetic field within the range of −15,000–15,000 Oe at room temperature. The magnetisation of $CoFe_2O_4$ MNP samples was not saturated by the SQUID (✗ Fig. 4). Therefore, the saturation magnetisation was obtained through extrapolation with a value of 7.5 emu/g [33].

3.5 EDX spectrum

EDX spectrum of $CoFe_2O_4$ MNPs shows the presence of elements of Fe, Co and O (Fig. 5). The peaks in the EDX pattern were perfectly assigned to the elements present in $CoFe_2O_4$ nanoparticles.

3.6 FTIR spectra

Fig. 6 shows the FTIR of $CoFe_2O_4$ MNPs. Two main bands at 590.31 and 416.35 cm^{-1} are assigned to M–O bond in octahedral and tetrahedral sites. 416.3 cm^{-1} is related to Co–O band and 590.3 cm^{-1} is associated with Fe–O band that confirmed the formation of $CoFe_2O_4$ in the sample. The FT-IR spectra showed

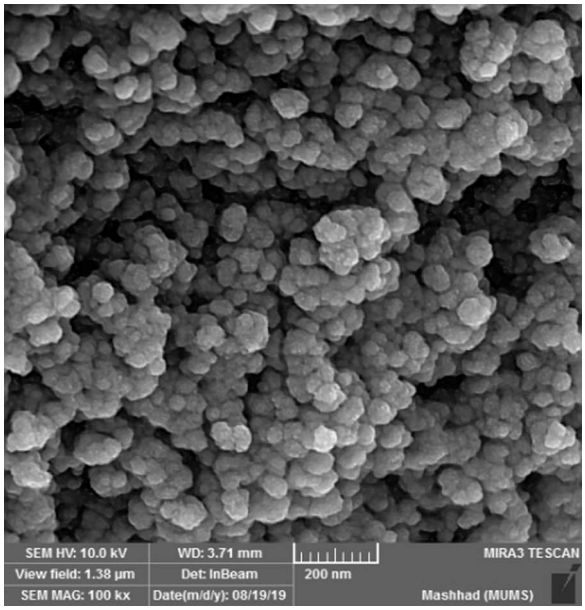

Fig. 3 *SEM images of $CoFe_2O_4$ MNPs. Size estimation was performed by imageJ software*

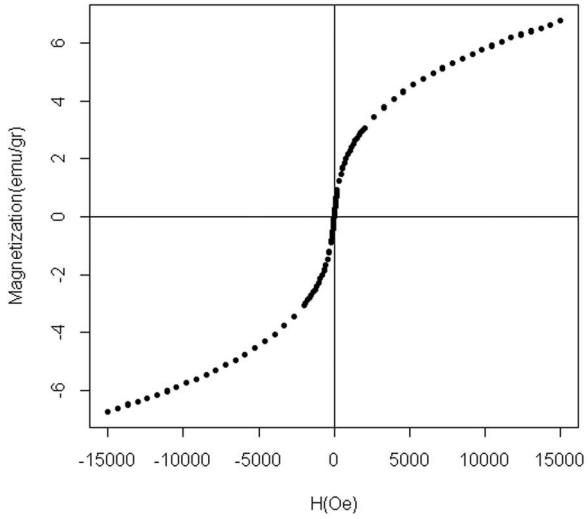

Fig. 4 *Magnetic hysteresis curves for $CoFe_2O_4$ MNPs. It was obtained at the magnetic field in the range of −15,000 to 15,000 Oe at the room temperature*

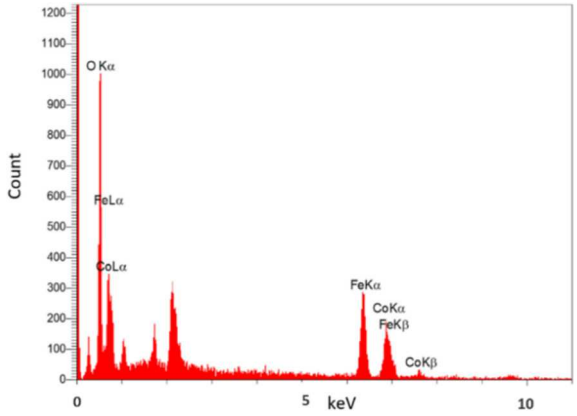

Fig. 5 *Energy dispersive X-ray spectroscopy (EDS or EDX) profile obtained from $CoFe_2O_4$ MNPs*

board bands at 3380 cm^{-1} which are related to the OH group on the surface of nanoparticles. The bands at 3414.3 and 1349.9 cm^{-1} are assigned due to the stretching of H–O–H bindings [34].

3.7 Relaxivity r_2

The MR capability of $CoFe_2O_4$ MNPs was tested using a 1.5 T MRI system. T_1 (longitudinal relaxation) and T_2 (transverse relaxation) are two independent relaxation processes to generate an MR image. In the presence of MNPs, the relaxation rate ($R = 1/T_{1,2}$) increases linearly with the MNPs concentration according to the following equation:

$$\frac{1}{T_{1,2}} = \frac{1}{T_0} + r_{1,2}C$$

where $1/T_0$ is the relaxation rate of pure water and C is the concentration of MNPs [35]. T_2 spin-echo multisection pulse sequence with fix TR of 2000 ms and different TEs ranging between 13.8 and 220 ms were acquired for T_2 measurement. Suspensions of $CoFe_2O_4$ MNPs at various concentrations (0.03–0.42 mM) were prepared in the DI water in 2 ml microtubes and DI water acted as controls in experiments. T_2 relaxation rates ($1/T_2$) were obtained by analysing the TE-dependent SI curve for various concentrations of $CoFe_2O_4$ MNPs (Fig. 7). T_2 weighted image of this nanostructure showed noticeable darkening by changing concentrations of MNPs in DI water. Thus, the SI of samples decreased at higher $CoFe_2O_4$ MNPs concentrations (Fig. 8*a*). The r_2 relativity was calculated as 58.6 mM^{-1} s^{-1} according to the linear plot slope of the $CoFe_2O_4$ MNPs concentration depending on the inverse T_2 with $R = 0.99$ (Fig. 8*b*).

3.8 Relaxivity r_1

Using the same token, r_1 was calculated by spin-echo with fix TE of 8.7 ms value and changing TR (from 100 to 2000 ms). T_1 weighted image of this MNPs showed low darkening by changing

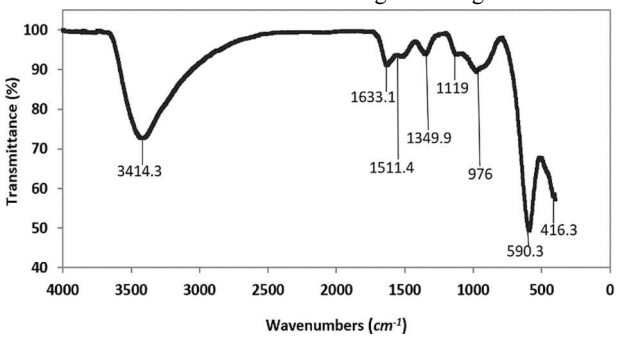

Fig. 6 *FTIR spectroscopy of $CoFe_2O_4$ MNPs*

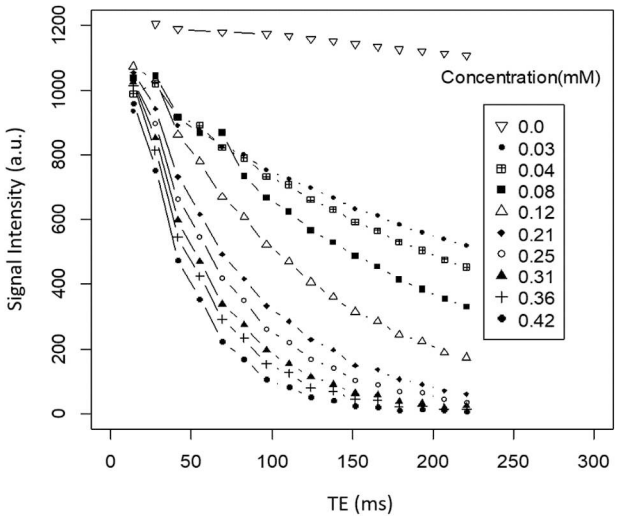

Fig. 7 *SI as a function of time of echo (TE) in various concentration of $CoFe_2O_4$ MNPs. Spin-echo multisection pulse sequence with fix time of repetition (TR) of 2000 ms and different TEs ranging between 13.8 and 220 ms for T_2 measurement at various concentrations (0.03–0.42 mM) that were prepared in the DI water and DI water played roles as a control sample*

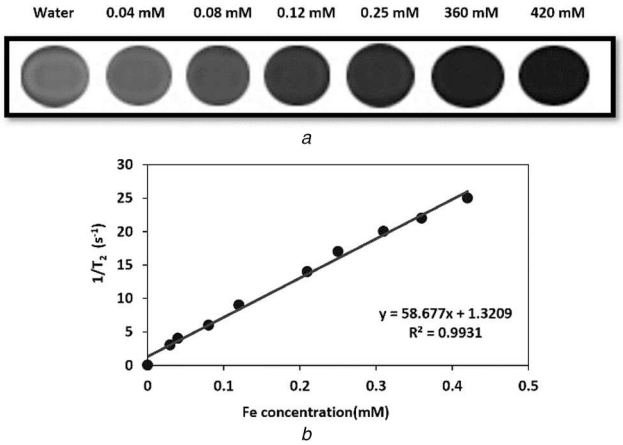

Fig. 8 *MR Image and calculated T_2 relaxation rates and relaxivity*

(a) T_2-weighted MR image of $CoFe_2O_4$ MNPs in water medium obtained by a conventional spin-echo pulse sequence on a 1.5 T MRI system, ***(b)*** T_2 relaxation rates ($1/T_2$) depending on the concentration, calculated T_2 relaxivity (r_2) at various Fe concentrations of (0.03 to 0.42 mM)

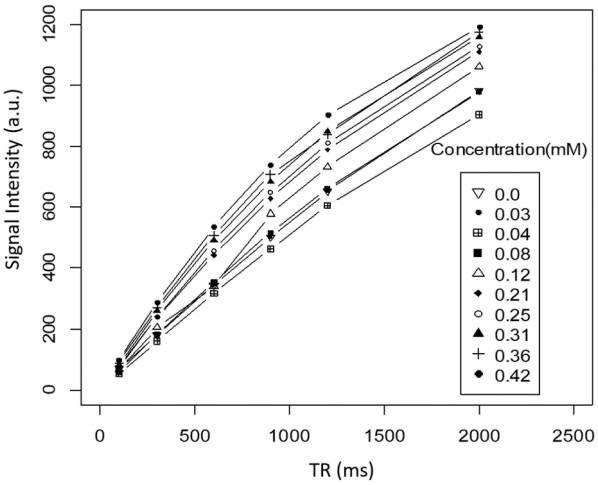

Fig. 9 *Spin echo sequence with fixed time of echo (TE) of 8.7 value and changing time of repetition (TR) (from 100 to 2000 ms) for T_1 measurement at various concentrations (0.03–0.42 mM) of $CoFe_2O_4$ MNPs that were prepared in the DI water*

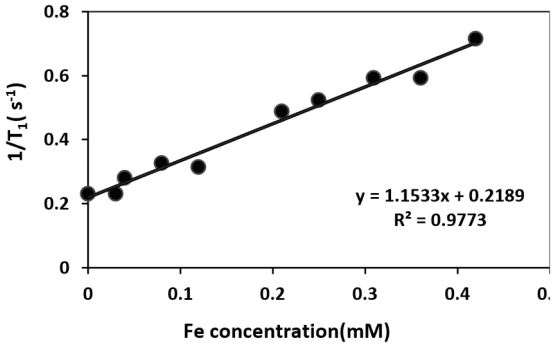

Fig. 10 *Calculated T_1 relaxation rates and relativity at 1.5 T with varying Fe concentration of $CoFe_2O_4$ MNPs (0.03 to 0.42 mM)*

Table 1 Changes in SI and percentage of ΔSI ((SI/$SI_{control}$) × 100) which $SI_{control}$ was related to cell phantom without MNPs) with concentration in cell phantoms image

Concentration, mM	Signal intensity	ΔSI, %
0	464	—
0.04	372	20
0.8	284	38
0.12	105	77
0.21	93.5	79
0.31	71.3	84

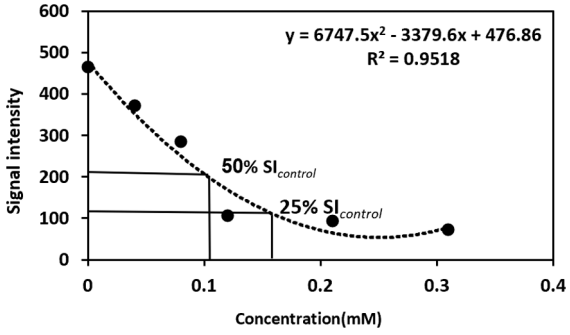

Fig. 11 *SI depended on concentration T_2- weighted MR image. 50 and 75% $SI_{control}$ accrue at concentrations of 0.87 and 0.154 mM, respectively*

concentrations of this MNPs (Fig. 9). According to Fig. 10, the longitudinal relaxation rate, r_1, was 1.15 $mM^{-1}s^{-1}$ for $CoFe_2O_4$ MNPs in DI water.

r_2/r_1 ratio: The r_2/r_1 ratio is an interesting sensitive parameter that is used to identify the category of the contrast agents (T_1 or T_2 contrast agent). The r_2/r_1 ratio was calculated as 51 in the present study.

3.9 In vitro MR imaging of cell phantom

To optimise the clinical application of $CoFe_2O_4$ MNPs, SI and ΔSI ((SI/$SI_{control}$) × 100) were obtained from cell phantom T_2 weighted image (✗ Table 1). The results indicated that the optimal concentration of $CoFe_2O_4$ MNPs was 0.154 mM to obtain 75% of maximum decay (Fig. 11).

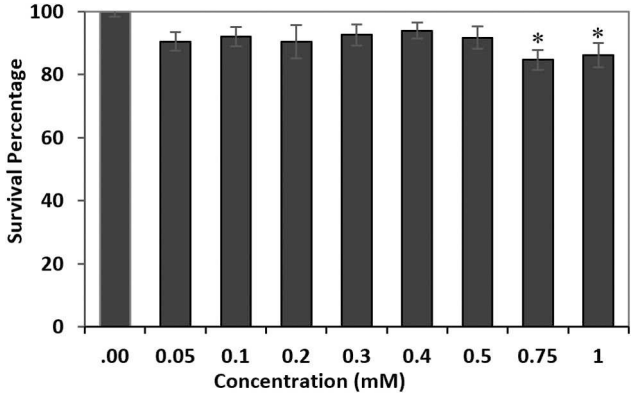

Fig. 12 *In vitro cytotoxicity of $CoFe_2O_4$ MNPs tested on KYSE 30 cell line for 24 h by MTT assay.The * sign indicates the significance of the statistic test*

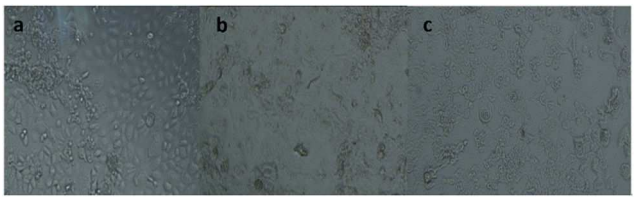

Fig. 13 *Morphology image of KYSE 30 cell*
(a) Without treatment (control), ***(b)*** Treated by 0.75 mM of $CoFe_2O_4$ MNPs, ***(c)*** Treated by 0.1 mM of $CoFe_2O_4$ MNPs

Cytotoxicity of $CoFe_2O_4$ MNPs: The cytotoxicity of $CoFe_2O_4$ MNPs was evaluated by analysing the cell survival MTT assay using KYSE30 cells. $CoFe_2O_4$ MNPs were incubated at various concentrations within the rage of 0.01–1 mM for 24 h. The test showed a survival rate of more than 80% for the maximum concentration of 1 mM (Fig. 12). Statistical analysis was performed by One-Way ANOVA test to compare control cells with the treated cells. Significant *p*-value was obtained by 0.009 and 0.028 for 0.75 and 1 mM of the MNPs concentrations, respectively. Morphology images of the treated KYSE30 cells with various concentrations of $CoFe_2O_4$ MNPs are shown in Fig. 13.

4 Discussion

This study aimed to synthesise and evaluate the performance of using superparamagnetic $CoFe_2O_4$ MNPs as a suitable T_2 contrast in clinical magnetic field strengths. Small size $CoFe_2O_4$ MNPs were synthesised through co-precipitation method that could be the result of using a good multifunctional agent. Relaxometry of $CoFe_2O_4$ MNPs, the optimal concentration of MNPs for MR imaging, and cytotoxicity effects of the MNPs were investigated.

HRTEM image of the synthesised $CoFe_2O_4$ MNPs shows a non-uniform and heterogeneous morphology. Also, there was an aggregation. Previous studies reported that smaller particles have a higher aggregation tendency due to lower energy barriers [36, 37]. The size distribution obtained from the HRTEM image revealed an average sizeof 10.45 nm for the synthesised MNPS. This size range was chosen for two reasons. Firstly, the superparamagnetic nanoparticles were characterised by size of <20 nm [38]. Secondly, MNPs smaller than 7 nm could not positively affect the r_2 relaxivity. However, slightly higher sizes could be optimal for the enhancement of the r_2 relaxivity [15, 17].

SAED pattern revealed that the synthesised sample is in polycrystalline nature (Fig. 2*c*). It shows dotted rings pattern corresponding to spinel cubic $CoFe_2O_4$ MNPs [31, 39, 40].

According to the SEM image, the synthesised MNPs showed non-uniform shape. Agglomeration of the MNPS could be the reason for higher size in SEM image that could be due to Van der Waals forces between the particles [41].

Through the analysis of XRD pattern, the crystal size of the synthesised $CoFe_2O_4$ MNPs (D) was estimated by theSherrer's equation with a small value of 11.67 nm. Subsequently, the lattice constant was estimated at 0.834 nm.

This finding is in agreement with the studies of Kalam*et al.* [42] and Houshiar *et al.* [1] indicating that the constant (a) of nanocrystalline depends on the size and synthesis method.

According to the hysteresis curve analysis of the $CoFe_2O_4$ MNPs, the lack of Hc and Mr refer to the superparamagnetic properties of the sample [33]. The small size effect and increased surface area of nanoparticles leading to superparamagnetic properties and the hysteresis curve without any loop [43]. The saturation magnetisation (M_S) of small-sized MNPs can be described by a magnetic-dead layer model.

It can be explained by the demagnetisation of surface spin due to the surface-to-volume ratio effect. According to this model, the reduced MNP size increased the surface-to-volume ratio, and thus the increased dead layer component decreased M_S [15].

After the characteristics of MNPs, MR images of $CoFe_2O_4$ MNPs were performed in an aqueous environment to evaluate the contrast between different concentrations of MNPs. T_2 weighted imaging of MNPs show a noticeable contrast by changing concentrations of MNPs. Therefore, $CoFe_2O_4$ MNPs could be considered as a negative contrast agent. Dephasing of the magnetic moment of protons could be caused by inhomogeneity in the magnetic field of environmental molecules in the presence of MNPs [44].

The r_2 value of $CoFe_2O_4$ MNPs was estimated at 58.6 by a magnetic relaxometry of $CoFe_2O_4$ MNPs suspension at a 1.5 T conventional MRI system. The r_2 value highly depends on size, M_S and the magnetic field strength [6]. The obtained r_2 was consistent with reports by Kang*et al.* indicating that T_2 relativity depends on the particle size, mass magnetisation and the concentration of MNPs [2, 45, 46]. The result was consistent with the study performed by Joos *et al.* [11] who proved that smaller MNPs, r_2 and r^*_2 decreased in a higher range of particle size because of the high surface spin anisotropy [47]. It was also consistent with the MAR theory. The size-dependent effect was strongly observable at low frequencies [15]. Consequently, the value of r_2 is related to small synthesised $CoFe_2O_4$ MNPs, low frequency and M_S that depended on the magnetic-dead layer. Despite these results, Venkatesha *et al.* [48] showed that with decreasing the size of $CoFe_2O_4$, an increase of r_2 could be achieved. This result could be due to many sharp edges on the surface of MNPs that leads to higher magnetic gradient.

Table 2 Some studies information using cobalt ferrite as a MRI contrast agent in aqueous medium

Reporter	Sample name	Size (nm) (TEM)	B, T	M_s, emu/g	r_1, $s^{-1}m\ M^{-1}$	r_2, $s^{-1}mM^{-1}$	$r2/r1$
Present study	$CoFe_2O_4$	10.5	1.5	7.5	1.15	58	51
Vamvakidis-2018 [35]	$CoFe_2O_4$ cluster	95 ± 12	1.5	116	0.2	3.1	14.8
Iatridi-2016 [62]	$MnFe_2O_4$:$CoFe_2O_4$-Copolymer	<100	1.5		1.85	39.87	21.55
Sitthichai-2017	$CoFe_2O_4$	20	1.5	40.36	—	1313	—
	$CoFe_2O_4$ coated DMSA	12	1.5	99	—	176	—
Venkatesha-2014	$CoFe_2O_4$	6,9,14	9.4	9.9, 34.2, 44.7	—	32, 2, 5	—
Liu-2013	$CoFe_2O_4$/H + /citrate	12.98–37.89	0.47	28.42–45.50	12.8–27.8	16.6–75.1	1.3–2.7
	$CoFe_2O_4$/H + /citrate	12.98–37.89	0.93		7.1–9.1	12.4–51	1.75–5.6
Cheongwon- 2013	$CoFe_2O_4$	10.5	4.7	—	—	66	—
	$CoFe_2O_4$@ SiO_2	15.8		—	—	179	—
		20		—	—	208	—
		24/2		—	—	302	—
		70.8				130	
Ravichandran- 2015	$CoFe_2O_4$ nanowhisker	40–90	7	74	2.367	256	108
Georgiadou-2015	$CoFe_2O_4$ -SBR	9–16	4	87	—	167.4	—

In this study, r_1 value was estimated at 1.15 mM^{-1} s^{-1}. The longitudinal relaxivity, r_1, was related to the dead layer of paramagnetic material by the free spin on the surface of NPs. r_1 also highly depended on the applied magnetic field. In this way, the increase of magnetic field strength decreases the value of r_1 [49, 50]. Some reports indicated that for MNPs of below 20 nm, r_1 increases with size [51].

The high value of r_2/r_1 ratio indicated T_2 contrast agent and vice versa [6, 52]. Some studies used cobalt ferrite as a contrast agent in the aqueous medium as shown in ✗ Table 2. According to the data of Table 2, the higher r_2/r_1 was achieved in large sizes of MNPs and high magnetic field values. In this study, the calculated high r_2/r_1 (51) compared to similar studies, indicated $CoFe_2O_4$ MNPs as a good candidate for a negative contrast agent in clinical magnetic field strength. The optimal concentrations of MNPs for MR image were calculated for the clinical applications. The research result indicated that higher concentrations of 0.154 mM of MNPs did not have any clinical value to obtain higher signal decay. Recent studies have found that MFe_2O_4 (M = Co, Ni, Cu or Zn) could induce the cytotoxicity and apoptosis by ROS generation and oxidative stress. The cytotoxicity of $CoFe_2O_4$ nanoparticles and risks for biological systems must be checked because of their widespread application [53–56]. Few research studies reported the toxic potential of cobalt MNPs [57, 58]. However, there are studies indicating the lack of toxicity of cobalt ferrite nanoparticles [59–61]. The cytotoxicity study of $CoFe_2O_4$ MNPs in this study indicated that concentrations of above 0.75 mM were toxic and the result agrees with the finding of Ravichandran *et al.* [14].

5 Conclusion

In this study, $CoFe_2O_4$ MNPs were synthesised by a co-precipitation method. It successfully produced approximately small superparamagnetic cobalt ferrite MNPs by the average size of 10.45 nm. T_1 and T_2 relaxation times of hydrogen protons in aqueous solutions of varying concentrations were determined with a conventional MRI. T_1 and T_2 relaxivities (r_1 and r_2) were determined to be 1.15 and 58 mM^{-1} s^{-1}, respectively. Owing to the high value of r_2/r_1 (51), this research demonstrated the potential use of the synthesised MNPs as appropriate negative contrast agents at the conventional MRI system at low applied concentration. In addition, our results suggest that the $CoFe_2O_4$ MNPs represent a perspective contrast agent suitable for cell labelling. The optimal concentration of $CoFe_2O_4$ MNP as an MR contrast agent was obtained at 0.154 mM which is within a non-toxic concentration range.

In vitro cell viability assays indicate that the $CoFe_2O_4$ MNPs showed no cellular viability reduction for concentrations up to 0.75 mM. As a result, it is suggested that this MNPs can be considered in further studies as a theranostic agent for improving the diagnostic and therapeutic application.

6 Acknowledgments

Results of this study were derived from a PhD thesis (Thesis #951622) in the Department of Medical Physics at Mashhad University of Medical Sciences. The work was financially supported by the Research Deputy of Mashhad University of Medical Sciences. The research did not receive any specific grant from other funding agencies in the public, commercial, or non-profit sectors.

7 References

[1] Houshiar, M., Zebhi, F., Razi, Z.J., *et al.*: 'Synthesis of cobalt ferrite ($CoFe_2O_4$) nanoparticles using combustion, coprecipitation, and precipitation methods: a comparison study of size, structural, and magnetic properties', *J. Magn. Magn. Mater.*, 2014, **371**, pp. 43–48

[2] Kang, J., Lee, H., Kim, Y.-N., *et al.*: 'Size-regulated group separation of $CoFe_2O_4$ nanoparticles using centrifuge and their magnetic resonance contrast properties', *Nanoscale Res. Lett.*, 2013, **8**, (1), p. 376

[3] Kherlopian, A.R., Song, T., Duan, Q., *et al.*: 'A review of imaging techniques for systems biology', *BMC Syst. Biol.*, 2008, **2**, (1), p. 74

[4] Sharma, P., Singh, A., Brown, S.C., *et al.*: 'Multimodal nanoparticulate bioimaging contrast agents', in '*Cancer nanotechnology*' (Humana Press, New Jersey, 2010), 624, pp. 67–81

[5] Venkatesha, N., Poojar, P., Ashwini, R., *et al.*: 'Ultrafine graphene oxide–$CoFe_2O_4$ nanoparticle composite as T_1 and T_2 contrast agent for magnetic resonance imaging', *RSC Adv.*, 2016, **6**, (21), pp. 17423–17429

[6] Rollet, A.-L., Neveu, S., Porion, P., *et al.*: 'New approach for understanding experimental NMR relaxivity properties of magnetic nanoparticles: focus on cobalt ferrite', *Phys. Chem. Chem. Phys.*, 2016, **18**, (48), pp. 32981–32991

[7] Zhang, M., Lu, J., Zhang, J.-N., *et al.*: 'Magnetic carbon nanotube supported Cu ($CoFe_2O_4$/CNT-Cu) catalyst: a sustainable catalyst for the synthesis of 3-Nitro-2-Arylimidazo [1, 2-a] pyridines', *Catal. Commun.*, 2016, **78**, pp. 26–32

[8] Özdinçer, M., Durmuş, S., Dalmaz, A.: 'Magnetic spinel-type $CoFe_2O_4$ nanoparticles: synthesis and investigation of structural, morphological properties', *Süleyman Demirel Üniversitesi Fen Bilimleri Enstitüsü Dergisi*, 2017, **21**, (2), pp. 311–315

[9] Colombo, M., Carregal-Romero, S., Casula, M.F., *et al.*: 'Biological applications of magnetic nanoparticles', *Chem. Soc. Rev.*, 2012, **41**, (11), pp. 4306–4334

[10] Hadera, H.T.: 'Iron oxide nanocrystals clustered in oil-in-water nanoemulsions: preparation, characterization, and transverse relaxivities'. NTNU, 2015

[11] Joos, A., Löwa, N., Wiekhorst, F., *et al.*: 'Size-dependent MR relaxivities of magnetic nanoparticles', *J. Magn. Magn. Mater.*, 2017, **427**, pp. 122–126

[12] Ta, H.T., Li, Z., Wu, Y., *et al.*: 'Effects of magnetic field strength and particle aggregation on relaxivity of ultra-small dual contrast iron oxide nanoparticles', *Mater. Res. Express*, 2017, **4**, (11), p. 116105

[13] Qin, J., Laurent, S., Jo, Y.S., *et al.*: 'A high-performance magnetic resonance imaging T_2 contrast agent', *Adv. Mater.*, 2007, **19**, (14), pp. 1874–1878

[14] Ravichandran, M., Oza, G., Velumani, S., *et al.*: 'Cobalt ferrite nanowhiskers as T_2 MRI contrast agent', *RSC Adv.*, 2015, **5**, (22), pp. 17223–17227

[15] Liu, F., Laurent, S., Roch, A., *et al.*: 'Size-controlled synthesis of $CoFe_2O_4$ nanoparticles potential contrast agent for MRI and investigation on their size-dependent magnetic properties', *J. Nanomater.*, 2013, **2013**, p. 127

[16] Georgiadou, V., Tangoulis, V., Arvanitidis, I., *et al.*: 'Unveiling the physicochemical features of $CoFe_2O_4$ NPs synthesized via a variant hydrothermal method: NMR relaxometric properties' *J. Phys. Chem. C.*, 2015, **119**, (15), pp. 8336–8348

[17] Menelaou, M., Iatridi, Z., Tsougos, I., *et al.*: 'Magnetic colloidal superparticles of Co, Mn and Ni ferrite featured with comb-type and/or linear amphiphilic polyelectrolytes; NMR and MRI relaxometry', *Dalton Trans.*, 2015, **44**, (24), pp. 10980–10990

[18] Mikalauskaitė, A., Kondrotas, R., Niaura, G., *et al.*: 'Gold-coated cobalt ferrite nanoparticles via methionine-induced reduction', *J. Phys. Chem. C*, 2015, **119**, (30), pp. 17398–17407

[19] Rajput, A.B., Hazra, S., Ghosh, N.N.: 'Synthesis and characterisation of pure single-phase $CoFe_2O_4$ nanopowder via a simple aqueous solution-based EDTA-precursor route', *J. Exp. Nanosci.*, 2013, **8**, (4), pp. 629–639

[20] Moreno, A.G., Guerrero, M.L., Alonso, E.V., *et al.*: 'Development of a new FT-IR method for the determination of iron oxide. Optimization of the synthesis of suitable magnetic nanoparticles as sorbent in magnetic solid phase extraction', *New J. Chem.*, 2017, **41**, (17), pp. 8804–8811

[21] Faghihzadeh, F., Anaya, N.M., Schifman, L.A., *et al.*: 'Fourier transform infrared spectroscopy to assess molecular-level changes in microorganisms exposed to nanoparticles', *Nanotechnol. Environ. Eng.*, 2016, **1**, (1), p. 1

[22] George, M., Nair, S.S., John, A.M., *et al.*: 'Structural, magnetic and electrical properties of the sol-gel prepared $Li_{0.5}Fe_{2.5}O_4$ fine particles', *J. Phys. D: Appl. Phys.*, 2006, **39**, (5), p. 900

[23] Duong, G.V., Turtelli, R.S., Hanh, N., *et al.*: 'Magnetic properties of nanocrystalline $Co_{1-x}Zn_xFe_2O_4$ prepared by forced hydrolysis method', *J. Magn. Magn. Mater.*, 2006, **307**, (2), pp. 313–317

[24] Phong, P., Phuc, N., Nam, P., *et al.*: 'Size-controlled heating ability of $CoFe_2O_4$ nanoparticles foráhyperthermia applications', *Phys. B*, 2018, **531**, pp. 30–34

[25] Zhao, S., Ma, D.: 'Preparation of $CoFe_2O_4$ Nanocrystallites by Solvothermal Process and Its Catalytic Activity on the Thermal Decomposition of Ammonium Perchlorate', *J. Nanomater.*, 2010, **2010**, (48), pp. 1–5

[26] Nabiyouni, G., Sharifi, S., Ghanbari, D., *et al.*: 'A simple precipitation method for synthesis $CoFe_2O_4$ nanoparticles', *J. Nanostruct.*, 2014, **4**, (3), pp. 317–323

[27] Shahjuee, T., Masoudpanah, S.M., Mirkazemi, S.M.: 'Coprecipitation synthesis of $CoFe_2O_4$ nanoparticles for hyperthermia', *J. Ultrafine Grained Nanostruct. Mater.*, 2017, **50**, (2), pp. 105–110

[28] Khodaei, M., Fayazzadeh, S.: 'Magnetic properties of $CoFe_2O_4$ nanoparticle synthesized by salt-assisted sol-gel auto-combustion method', *Mater. Res. Express*, 2019, **6**, (8), p. 086115

[29] Ramalho, M., Gama, L., Antonio, S., *et al.*: 'X-ray diffraction and Mössbauer spectra of nickel ferrite prepared by combustion reaction', *J. Mater. Sci.*, 2007, **42**, (10), pp. 3603–3606

[30] Hedayati, K., Azarakhsh, S., Ghanbari, D.: 'Synthesis and magnetic investigation of cobalt ferrite nanoparticles prepared via a simple chemical precipitation method', *J. Nanostruct.*, 2016, **6**, (2), pp. 127–131

[31] Darwish, M.S., Kim, H., Lee, H., *et al.*: 'Synthesis of magnetic ferrite nanoparticles with high hyperthermia performance via a controlled co-precipitation method', *Nanomaterials*, 2019, **9**, (8), p. 1176

[32] Chandekar, K.V., Mohan Kant, K.: 'Synthesis and characterization of low temperature superparamagnetic cobalt ferrite nanoparticles', *Adv. Mater. Lett.*, 2017, **8**, (4), pp. 435–443

[33] Alsmadi, A., Bsoul, I., Mahmood, S., *et al.*: 'Magnetic study of M-type doped barium hexaferrite nanocrystalline particles', *J. Appl. Phys.*, 2013, **114**, (24), p. 243910

[34] Vinosha, P.A., Mely, L.A., Mary, G.I.N., *et al.*: 'Study on cobalt ferrite nanoparticles synthesized by co-precipitation technique for photo-Fenton application', *Mech. Mater. Sci. Eng. J.*, 2017, **9**, (1), pp. 110–115

[35] Vamvakidis, K., Mourdikoudis, S., Makridis, A., *et al.*: 'Magnetic hyperthermia efficiency and MRI contrast sensitivity of colloidal soft/hard ferrite nanoclusters', *J. Colloid Interface Sci.*, 2018, **511**, pp. 101–109

[36] Marimón-Bolívar, W., González, E.E.: 'Study of agglomeration and magnetic sedimentation of glutathione@ Fe_3O_4 nanoparticles in water medium', *Dyna*, 2018, **85**, (205), pp. 19–26

[37] Gambinossi, F., Mylon, S.E., Ferri, J.K.: 'Aggregation kinetics and colloidal stability of functionalized nanoparticles', *Adv. Colloid Interface Sci.*, 2015, **222**, pp. 332–349

[38] Ishizaki, T., Yatsugi, K., Akedo, K.: 'Effect of particle size on the magnetic properties of Ni nanoparticles synthesized with trioctylphosphine as the capping agent', *Nanomaterials*, 2016, **6**, (9), p. 172

[39] Qasim, M., Asghar, K., Das, D.: 'Preparation and characterization of $CoFe_2O_4$ and $CoFe_2O_4$@ albumen nanoparticles for biomedical applications', *Ceram. Int.*, 2019, **45**, (18), pp. 24971–24981

[40] Saccone, F.D., Ferrari, S., Errandonea, D., *et al.*: 'Cobalt ferrite nanoparticles under high pressure', *J. Appl. Phys.*, 2015, **118**, (7), p. 075903

[41] Joseph, A.M., Thangaraj, B., Gomathi, R.S., *et al.*: 'Synthesis and characterization of cobalt ferrite magnetic nanoparticles coated with polyethylene glycol', *AdvNanoBioM&D.*, 2017, **1**, (1), pp. 71–77

[42] Kalam, A., Al-Sehemi, A.G., Assiri, M., *et al.*: 'Modified solvothermal synthesis of cobalt ferrite ($CoFe_2O_4$) magnetic nanoparticles photocatalysts for degradation of methylene blue with H_2O_2/visible light', *Results Phys.*, 2018, **8**, pp. 1046–1053

[43] Theivasanthi, T., Alagar, M.: 'Innovation of superparamagnetism in lead nanoparticles', arXiv preprint arXiv:1402.1431, 2014

[44] Zhou, Z., Tian, R., Wang, Z., *et al.*: 'Artificial local magnetic field inhomogeneity enhances T_2 relaxivity', *Nat. Commun.*, 2017, **8**, (1), pp. 1–10

[45] Jun, Y.-W., Huh, Y.-M., Choi, J.-S., *et al.*: 'Nanoscale size effect of magnetic nanocrystals and their utilization for cancer diagnosis via magnetic resonance imaging', *J. Am. Chem. Soc.*, 2005, **127**, (16), pp. 5732–5733

[46] Shapiro, E.M., Skrtic, S., Sharer, K., *et al.*: 'MRI detection of single particles for cellular imaging', *Proc. Natl. Acad. Sci.*, 2004, **101**, (30), pp. 10901–10906

[47] Issa, B.: 'Reduction of T_2 relaxation rates due to large volume fractions of magnetic nanoparticles for all motional regimes', *Appl. Sci.*, 2018, **8**, (1), p. 101

[48] Venkatesha, N., Srivastava, C., Hegde, V.: 'Synergetic effect of size and morphology of cobalt ferrite nanoparticles on proton relaxivity', *IET Nanobiotechnol.*, 2013, **8**, (4), pp. 184–189

[49] Rohrer, M., Bauer, H., Mintorovitch, J., *et al.*: 'Comparison of magnetic properties of MRI contrast media solutions at different magnetic field strengths', *Invest. Radiol.*, 2005, **40**, (11), pp. 715–724

[50] Weerakoon, B.S., Osuga, T., Konishi, T.: 'Enhancement effect of superparamagnetic iron oxide nanoparticle-based MRI contrast agent at different concentrations and magnetic field strengths', *World Academy of Sci. Eng. Technol. Int. J. Chem. Mol. Nuclear, Mater. Metallurgical Eng.*, 2016, **10**, (1), pp. 50–53

[51] Davies, G.L., Corr, S.A., Meledandri, C.J., *et al.*: 'NMR relaxation of water in nanostructures: analysis of ferromagnetic Cobalt–Ferrite polyelectrolyte nanocomposites', *ChemPhysChem*, 2011, **12**, (4), pp. 772–776

[52] Issa, B., Obaidat, I.M., Albiss, B.A., *et al.*: 'Magnetic nanoparticles: surface effects and properties related to biomedicine applications', *Int. J. Mol. Sci.*, 2013, **14**, (11), pp. 21266–21305

[53] Thunus, L., Lejeune, R.: 'Overview of transition metal and lanthanide complexes as diagnostic tools', *Coord. Chem. Rev.*, 1999, **184**, (1), pp. 125–155

[54] Sijens, P.E., Van Den Bent, M.J., Nowak, P.J., *et al.*: '1 h chemical shift imaging reveals loss of brain tumor choline signal after administration of Gd-contrast', *Magn. Reson. Med.*, 1997, **37**, (2), pp. 222–225

[55] Chang, C.A.: 'Magnetic resonance imaging contrast agents design and physicochemical properties of gadodiamide', *Invest. Radiol.*, 1993, **28**, pp. S21–S27

[56] Xiao, Y.-D., Paudel, R., Liu, J., *et al.*: 'MRI contrast agents: classification and application', *Int. J. Mol. Med.*, 2016, **38**, (5), pp. 1319–1326

[57] Naqvi, S., Samim, M., Abdin, M., *et al.*: 'Concentration-dependent toxicity of iron oxide nanoparticles mediated by increased oxidative stress', *Int. J. Nanomed.*, 2010, **5**, p. 983

[58] Huang, G., Chen, H., Dong, Y., *et al.*: 'Superparamagnetic iron oxide nanoparticles: amplifying ROS stress to improve anticancer drug efficacy', *Theranostics*, 2013, **3**, (2), p. 116

[59] Ahmad, F., Liu, X., Zhou, Y., *et al.*: 'An in vivo evaluation of acute toxicity of cobalt ferrite ($CoFe_2O_4$) nanoparticles in larval-embryo Zebrafish (Danio Rerio)', *Aquat. Toxicol.*, 2015, **166**, pp. 21–28

[60] Song, M.-M., Song, W.-J., Bi, H., *et al.*: 'Cytotoxicity and cellular uptake of iron nanowires', *Biomaterials*, 2010, **31**, (7), pp. 1509–1517

[61] Cao, J., Liu, Y., Jia, L., *et al.*: 'Curcumin attenuates acrylamide-induced cytotoxicity and genotoxicity in HepG2 cells by ROS scavenging', *J. Agric. Food Chem.*, 2008, **56**, (24), pp. 12059–12063

[62] Iatridi, Z., Vamvakidis, K., Tsougos, I., *et al.*: 'Multifunctional polymeric platform of magnetic ferrite colloidal superparticles for luminescence, imaging, and hyperthermia applications', *ACS Appl. Mater. Interfaces*, 2016, **8**, (51), pp. 35059–35070